Surface Review and Letters, Vol. 29, No. 7 (2022) 2250093 (13 pages)

DOI: 10.1142/S0218625X22500937

World Scientific
www.worldscientific.com

INVESTIGATION ON THE THERMAL BEHAVIOR OF FRICTION STUD WELDING OF DISSIMILAR ALUMINUM/MILD STEEL JOINTS

R. THARMARAJ[*,‡] and N. RAJESH JESUDOSS HYNES[†,§]
[*]*Institute of Fundamental Technological Research,*
Polish Academy of Sciences,
Pawińskiego 5B, Warsaw 02-106, Poland

[†]*Department of Mechanical Engineering,*
Mepco Schlenk Engineering College,
Sivakasi, Tamilnadu 626005, India
[‡]*tharmaraj88@yahoo.com*
[§]*findhynes@yahoo.co.in*

Received 8 January 2022
Revised 22 March 2022
Accepted 23 April 2022
Published 13 June 2022

Friction stud welding process is a suitable candidate in joining stud fasteners for steel structure buildings, military vehicles, automobiles, aircraft, ocean liners, bridges, ship buildings, etc., The peak temperature for welding is achieved by converting mechanical energy to thermal energy at the sample interface without the use of electric energy from other sources because it is a solid-state process. The study of the thermal behavior of different metals during friction stud welding is very important since it is a thermal energy process. However, there is no good thermal model for the friction stud welding process. In this work, the generation of heat flux at the interfacial area of two distinct metals, namely aluminum and mild steel, is calculated using a mathematical model. The temperature at the interfacial region, which plays a significant role in the quality and strength of the weld component, is particularly focused on experimentation and analytical modeling. In the experimentation, a noncontact type infrared thermometer is used to measure temperature directly. The temperature profile was determined by the finite difference method based on thermal resistance and capacitance formulation at transient conditions. The obtained mathematical results are compared with the experimental results at the distance of 5 and 10 mm from the welded interface. The computed temperature profile is in good agreement with the experimental data on the heating side and with a minimum degree of deviation in the cooling part. The maximum percentage of error for the 5 mm interface is 3.349 and for the 10 mm interface is 2.857. This deviation is due to the zero-axial shortening assumption in the analytical model. Besides, the temperature characteristics of the welded are analyzed at various time increments by numerical simulation. As a result, the predicted temperature is more on the aluminum side compared to the mild steel due to a change in thermal properties. This proposed thermal model would be helpful to improve the design and manufacture of welding machines.

Keywords: Friction stud welding; thermal modeling; finite difference method; numerical simulation; aluminum; mild steel.

[§]Corresponding author.

1. Introduction

Welding is an important fabrication process that is commonly used to join two or more parts that are bonded together by the application of heat, pressure, or both developing new welded parts. During the welding of different materials, the evolution of intermetallic in the weld zone reduces the toughness and structural reliability of the joint.[1–3] The butt-welding technique has a variety of flaws connected with the joining of incompatible metals. The most common issues with weld beads are fusion zone, transverse, and longitudinal flaws.[4] As a result, standard welding procedures are not thought to be a viable option for dissimilar joints.[5] Friction stud welding is a modification of friction stir welding (FSW) originally developed to fusion weld Al-alloys.[6–12] Similar to FSW, friction stud welding is also classified as a solid-state welding technique, in which welding occurs at a temperature below the melting point of the work metal. Welds are made by holding a nonrotating stud in contact with a rotating workpiece under slowly growing pressure until the interface reaches the joining temperature and then stopping rotation to finish the weld. Friction welding (FW) does not produce the typical flaws associated with melting and solidification found in traditional welding techniques, such as porosity.[13,14] The friction mechanism in the FW process converts mechanical energy to heat energy, melting the metal's surfaces, and compression force aid in connecting the metals.[15] The FW process has several advantages, including a narrow heat-affected zone, reduced porosity, slag inclusion and undercut solute redistribution, and solidification cracking.[16] Because of these qualities, FW can be used to weld incompatible materials. Various groupings of dissimilar metals have been successfully experienced up till now, such as aluminum/copper, aluminum/steel and titanium/steel.[17–19] Aluminum and steel alloys have recently received more attention due to their wide range of industrial applications.[20] But it is relatively challenging to joint two dissimilar metals due to their mechanical and thermal properties.[21] As a result, it is critical to examine the thermal behavior and temperature distribution in friction stud welding of aluminum (Al) and mild steel (MS).

One of the most essential aspects of friction stud welding analysis is heat transport. Predicting the thermal cycles in the welding workpiece and evaluating the weld quality may be easier with a basic grasp of heat transport. Several studies have found that the heat transfer in FW has a direct impact on the quality of the welded joints.[22] Heat is focused on the joint interface in welded joints, and the size of the heat-affected zone determines the joint's qualities. Therefore, the researchers have analyzed the thermal characteristics of the mechanical features of two dissimilar Al and MS combinations.[23] They observed that the hardness and tensile strength of the welded components are affected due to the thermal effects during the process. In recent years, different authors have developed a thermal model for predicting the thermal history of different dissimilar joints, such as AA7075-AA2014, AA5005-ASTM A248 steel, hardenable Al alloys, Al–Al, Al–steel, and Al–copper using the FSW process.[24–28] The researchers compared the temperature profile results and the microstructure in the joint contact are quite similar to the experimental results.[24] The peak temperature and cooling rate are reduced during underwater treatment, resulting in a smooth surface with minimal surface oxidation.[25] The developed thermal model predictions revealed that the hardness values are affected by the amount of heat applied and the welding speed.[26] The thermal histories that resulted were used to calculate the growth of intermetallic phases at the Al–steel weld joint.[27] Before experimenting, numerical modeling anticipated the influence of various variables on the temperature profile of dissimilar alloys.[28] An overview of the thermal behavior of friction welded joints reveals that the established thermal models can be used to estimate weld quality in practice.

According to the wide literature, various researchers have examined the thermal behavior of friction welded dissimilar metals.[29–33] In the literature, however, the impact of process parameters on the thermal behavior of friction stud welded joints of dissimilar metal have not been properly explored. Moreover, the investigation of the thermal characteristics of various parts during friction stud welding is very significant since it is a thermal energy process, yet there is no good thermal model for the friction stud welding process. Therefore, thermal modeling of the friction stud welding process has been performed for the dissimilar Al and MS combination.[34–42] Friction stud welding of Al and MS joints is carried out by varying the process

parameters of frictional time, frictional pressure, rotational speed, forging pressure, and forging time. These parameters determine the amount of energy input to the welded joint and the generation of heat rate at the interface. The generation of heat during friction stud welding is calculated by using the micro-annulus heat generation model. The highest joint temperature and temperature contour in the area near the joint can have a significant impact on the flash formation, heat-affected zone, and joint strength. Cooling rates are closely related to joint temperature profiles and they directly influence the residual stress state established in the weld. Hence, it is vital to have means of rapidly and accurately estimating the highest weld temperature and cooling rate based on input parameters. The distribution of temperature is measured experimentally and also calculated using the thermal resistance and capacitance formulation of the finite difference method (FDM). The finite element simulation helps in better understanding of the friction stud welding method and it is significant to compute the temperature during the welding process.

2. Experimental Details

Aluminum and steel-based combinations have been gaining popularity in several industrial sectors over the last few decades due to their lightweight, superior corrosion resistance, and high mechanical strength.[43–46] Therefore, aluminum (Al) and mild steel (MS) materials were chosen for examination in this study. Table 1 shows their chemical compositions and the properties of both of the materials used in this study. The thermal conductivity of both metals varies with respect to the temperature. Table 2 gives the values of thermal conductivity at different temperatures.

The friction stud welding is carried out in four phases. The rotational specimen is subjected to an axial load in the first phase, and the two parts are taken close to the welded surfaces. Frictional heating occurs at the interfaces of the two samples in the next

Table 1. Chemical composition and properties of Al–MS.

Chemical composition		Properties	
MS	Al	MS	Al
Fe: 98 C: 0.30 Mn: 0.78 Si: 0.22 Ni: 0.10 Cr: 0.12 Mo: 0.50 P: 0.02 S: 0.02 Cu: 0.44	Cu: 0.25 Mg: 0.85 Si: 0.59 Fe: 0.22 Zn: 0.03 Mn: 0.09 Ni: 0.01 Al: 98	Density: 7833 Kg/m^3 Thermal diffusivity: $14.74 \times 10^{-6}\, m^2/s$ Specific heat: 465 J/kgK	Density: 2707 Kg/m^3 Thermal diffusivity: $84.18 \times 10^{-6}\, m^2/s$ Specific heat: 896 J/kgK

Table 2. Thermal conductivity of Al and MS at different conditions.

Temperature (°C)	Thermal conductivity of MS (W/mK)	Thermal conductivity of Al (W/mK)
0	55.40	202.50
100	51.90	206.00
200	48.50	214.60
300	45.00	228.20
400	41.50	249.20

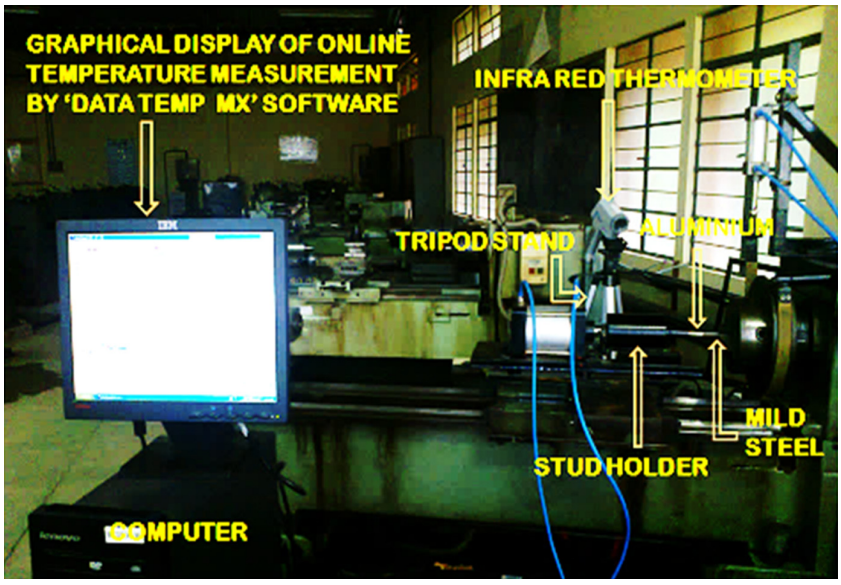

Fig. 1. Experimental set-up for online temperature measurement.

stage. When the rotational speed is stopped in the third phase, upsetting occurs repeatedly under tremendous pressure. The pressure is still the same until the axial pressure is removed in the last step. The group of operational parameters such as friction pressure (300 kPa), friction time (6 s), forging time (8 s), forging pressure (500 kPa), and rotational speed (1600 rpm) are preferred for the friction stud welding. Experiments are carried out in a direct-drive friction stud welding machine with a programmable logic controller. During the process of friction stud welding, the online temperature measurement has been carried out using a noncontact infrared thermometer connected to a computer via a data logger as shown in Fig. 1. Interactive software "Data Temp MX (v 1.12)" is used to generate thermal profiles during the welding process in real-time. During the process, Al acts as a sliding component and MS acts as a rotating component. The diameter and length of the workpiece for both the material are 12 and 45 mm, respectively. A successful welded Al–MS specimen is shown in Fig. 2.

Fig. 2. Friction stud welded Al–MS specimen.

3. Thermal Modeling of Friction Stud Welding

Friction stud welding is a thermal energy process. Despite the fact that there are several thermal models for FW approaches, there is none for the friction stud welding method. The generation of heat flow at the interfacial region of the two different metals is predicted by a mathematical model. Heat loss via radiation is expected to be small, and heat transmission from the tip of the short, narrow cylindrical workpiece is assumed to be nil.

3.1. *Need for modeling*

Because the entire process takes place in such a short amount of time, the heat transfer analysis is the most significant part of the friction stud welding process study. A thorough understanding of the workpiece's heat transfer mechanism can aid in forecasting the welding operation's thermal cycles. It can also be used to anticipate the hardness, strength, and weld quality of the weld zone. Furthermore, when modeling material flow, a known temperature distribution is critical for computing temperature-dependent viscosity. By changing the input power, the temperature

distribution across the interface can be altered to a large extent. The work required to break down metallic connections created at the friction surface generates heat in friction stud welding. As metallic bonds break down, the temperature of the metal at the welding joint's interfacial region rises. This minimizes the amount of energy required to break down freshly established connections, causing heat to be generated where the contact to be disrupted. Many researchers were able to explain the differential heat flow calculations for the appropriate boundary settings by employing heat conduction theory, ensuring that expectations are simplified, and assessing the many steps of the process. Cheng evaluated the temperature distribution of steel during FW using a finite difference approach.[29,30] Despite all of this research, there is currently no adequate heat flow model for friction stud welding. This state is caused by a complicated set of responses resulting from the interaction of several variables that are difficult to account for in a mathematical simulation of the process.

Rykalin's infinite rod assumption is used in all existing thermal models. Rykalin's model analyzes a long rod with a constant heat source. Starting when time (t) is 0, heat is released at a steady rate. Rykalin considers the welded joint to be an infinitely long rod. Although this assumption is valid for the FW process, it is less so for the friction stud welding process, because the stud to be welded is not the same as a typical component to be welded. The stud is usually a thin cylindrical rod with a small diameter and length that resembles a pin fin. As a result, an appropriate thermal model for the friction stud welding process must be developed, with certain adjustments. The joining of dissimilar metals is studied in this paper, and the studs are just treated as a shortfin in the thermal analysis.

3.2. *Analytical modeling of heat generation*

The frictional heat was calculated using the following analytical approach, assuming that the force distribution remained constant. First, in the friction surface, a micro-annulus with an inner radius r and a width dr is defined as shown in Fig. 3. The constant pressure acting on the entire surface is given by p. The area of the micro-annulus is $dA = 2\pi r dr$. Transforming the pressure equation into a differential

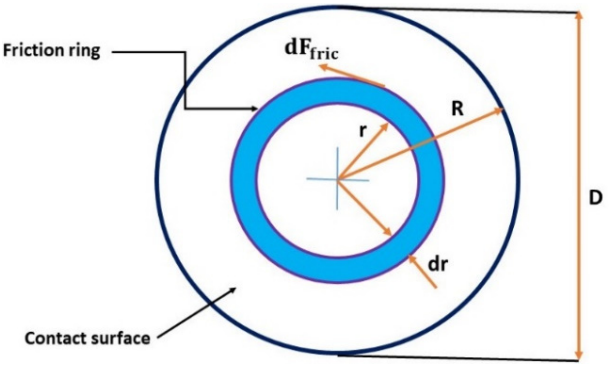

Fig. 3. (Color online) Micro-annulus heat generation model.

characterization of the area dA, the following equation is obtained for the differential force, dF, acting on the area dA.

$$dF = pdA = 2p\pi r dr. \tag{1}$$

Since dF is equivalent to the equal and opposite normal force acting on dA, the differential frictional force, dF_{fric} can be specified as

$$dF_{\text{fric}} = \mu dF = 2\mu p\pi r dr, \tag{2}$$

where μ is friction coefficient. It is known that the tangential velocity, V_T, at any point on the element is the same

$$V_{\text{T}} = r\omega, \tag{3}$$

where ω is the angular velocity

$$\omega = \frac{2\pi N}{60}, \tag{4}$$

where N is the rotational speed. The differential power that is exerted to rotate the annulus area dA is

$$dP = dF_{\text{fric}} V_T = 2\mu p\pi r^2 \omega \text{dr}. \tag{5}$$

The heat flux (q) generated by friction at the annulus is given as

$$q = \frac{dP}{dA} = \mu pr\omega. \tag{6}$$

3.3. *Simple pin fin model*

The proposed basic pin fin model for the friction stud welding process is given in Fig. 4. All existing thermal models are compatible with the FW process because they are based on Rykalin's infinite rod assumption.

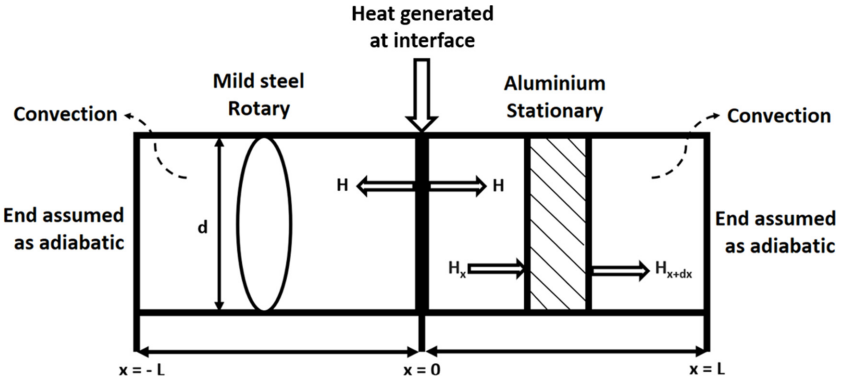

Fig. 4. Simple pin fin model for friction stud welding process.

The stud, however, is a thin cylindrical rod with a small diameter that resembles the shape of a pin fin, and the existing models are insufficient for the friction stud welding process. The joining of Al and MS is taken into account in this study, and the studs are merely treated as a shortfin in the thermal analysis. The component is modeled as a narrow cylindrical rod with an adiabatic end and no axial shortening in the friction stage, comparable to a pin fin.

3.4. *Finite difference-based pin fin model*

The pin fin model is integrated into an FDM technique to perform transient analysis. Thermal resistance–capacitance formulation can be used to solve the explicit technique of formulation for the FDM. The resistance–capacitance formulation was chosen because it was simple to adjust to changes in thermal properties as a function of temperature. The following equation governs the finite difference equations for unsteady–state conduction problems:

$$\frac{\partial^2 \mathrm{T}}{\partial^2 \mathrm{x}} = \frac{1}{\propto} \frac{\partial \mathrm{T}}{\partial \mathrm{t}}. \tag{7}$$

Forwarding, backward and central operators can be used to estimate the time derivative. The explicit technique is used to solve forward difference approximations for finite difference equations. The temperature $(\mathrm{Ti})^{n+1}$ is calculated as a result of an explicit evolution. The net energy transfer into the node is zero during steady-state conditions, but it must be demonstrated as an increase in the element's internal energy under unsteady–state situations. Each volume element (ΔV) acts as a small "lumped capacity" and the solid's behavior during a temporary process is determined by the interaction of all the elements. The thermal effect might be computed for each node by providing appropriate inputs of material attributes such as density (ρ), specific heat (c), and thermal conductivity (k). It may be essential to measure new values of thermal capacitance (C_i) and thermal resistance (R_{ij}) for each iteration, depending on the nature of the problem and the level of precision required. Figure 5 depicts the FDM of the friction stud welding process. The stud is a thin cylindrical rod with a tiny diameter, and heat generation at the interface is expected to be constant. The list of the steps involved in the FDM of the friction stud welding process is given in the following.

Step 1: Construction of the grid for each node

The grid construction for every node in FDM is shown in Fig. 6. The node numbers are taken as 0, 1, 2, 3, 4, 5 and 6. The distance between two nodes is taken as Δx and it is measured from the length of the specimen. The total length of each specimen is 45 mm. Node 0 is a central node, nodes 1, 2, 4 and 5 are the interior nodes, nodes 3 and 6 are the exterior nodes.

Step 2: Thermal resistance and capacitance formulation

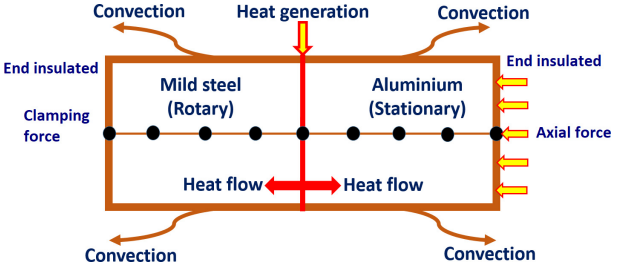

Fig. 5. (Color online) Finite difference model of friction stud welding.

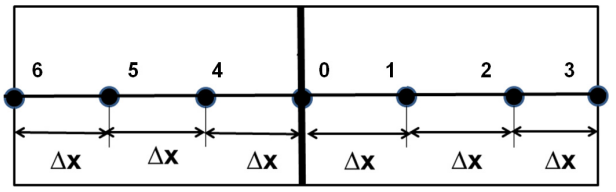

Fig. 6. Construction of the grid in FDM.

The thermal resistance and capacitance are calculated by the following equation. Thermal resistance and capacitance for the interior nodes are calculated by the following expression:

$$\mathrm{TR}_{m+} = \mathrm{TR}_{m-} = \frac{\Delta x}{kA}, \tag{8}$$

$$\mathrm{TR}_{\infty} = \frac{1}{h(\pi d \Delta x)}, \tag{9}$$

$$\mathrm{TC}_i = \rho c \Delta V, \tag{10}$$

where TR_{m+} and TR_{m-} are the thermal resistance of interior nodes in the forward and backward direction, TR_{∞} is the thermal resistance of interior nodes due to convection, Δx is the distance between two nodes, k is the thermal conductivity of the material, A is the area of the specimen, h is the convective heat transfer coefficient, d is the diameter of the specimen, ρ is the density of the material, c is the specific heat of the material and ΔV is the volume of the element.

Similarly, the thermal resistance and capacitance of the exterior nodes are calculated by the following expression:

$$\mathrm{TR}_{m+} = \frac{1}{hA}, \tag{11}$$

$$\mathrm{TR}_{m-} = \frac{\Delta x}{kA}, \tag{12}$$

$$\mathrm{TR}_{\infty} = \frac{2}{h(\pi d \Delta x)}, \tag{13}$$

$$\mathrm{TC}_i = \frac{\rho c \Delta V}{2}. \tag{14}$$

The nodal resistances in various situations are shown in Table 3.

Step 3: Determination of temperature

For the calculation of nodal temperature by iteration, the following stability criterion is employed:

$$\Delta\tau \leq \left[\frac{\mathrm{TC}_i}{\sum \frac{1}{\mathrm{TR}_{ij}}}\right] \min, \tag{15}$$

where $\Delta\tau$ is the stability criteria, TC_i is the thermal capacitance and it is calculated by using Eqs. (10) and (14). TR_{ij} is the thermal resistance of the ith and jth node. For each node the formulation of $\sum \frac{1}{\mathrm{TR}_{ij}}$ is

$$\sum \frac{1}{\mathrm{TR}_{ij}} = \frac{1}{\mathrm{TR}_{m+}} + \frac{1}{\mathrm{TR}_{m-}} + \frac{1}{\mathrm{TR}_{\infty}}. \tag{16}$$

The temperature distribution with various time increments is calculated by the following explicit formulation technique:

$$T_i^{p+1} = \frac{\Delta\tau}{\mathrm{TC}_i}\left[q_i + \sum \frac{T_j^p - T_i^p}{\mathrm{TR}_{ij}}\right] + T_i^p, \tag{17}$$

where T_i^{p+1} is the temperature of the ith node for a future time, T_i^p is the temperature of an ith node in the present time, T_j^p is the temperature of a jth node in the present time, TR_{ij} is the thermal resistance of the ith and jth node and it is calculated by Eq. (16). $\Delta\tau$ is the stability criteria determined by Eq. (15), TC_i is the thermal capacitance, calculated by using Eqs. (10) and (14), q_i is the heat generation, determined by Eq. (6).

Table 3. Resistance for nodes.

Physical situation	TR_{m+}	TR_{m-}	ΔV
Interior node	$1/k$	$1/k$	$(\Delta x)^2$
Convection boundary	$1/h\Delta x$	$1/k$	$(\Delta x)^{2/2}$
Exterior corner, convection	$2/h\Delta x$	$2/k$	$(\Delta x)^{2/4}$
Interior corner, convection	$2/k$	$1/k$	$3(\Delta x)^{2/4}$
Insulated boundary	∞	$1/k$	$(\Delta x)^{2/2}$

4. Results and Discussion

4.1. *Experimental results*

Figure 1 depicts the investigative setup for online temperature measurement. The noncontact infrared thermometer's spot size can be focused on the weld joint interface. Figure 7 shows the computed data during the research shown against time using Data Temp MX. A large amount of heat is created in the interfacial area during friction stud welding process. A noncontact type infrared thermometer is used to calculate temperature changes during the process at the interfacial district. A data recorder is incorporated into the infrared thermometer, which is connected to a dedicated computer for online measurement. During the experimentation, the rotating speed, friction pressure, friction time, forging

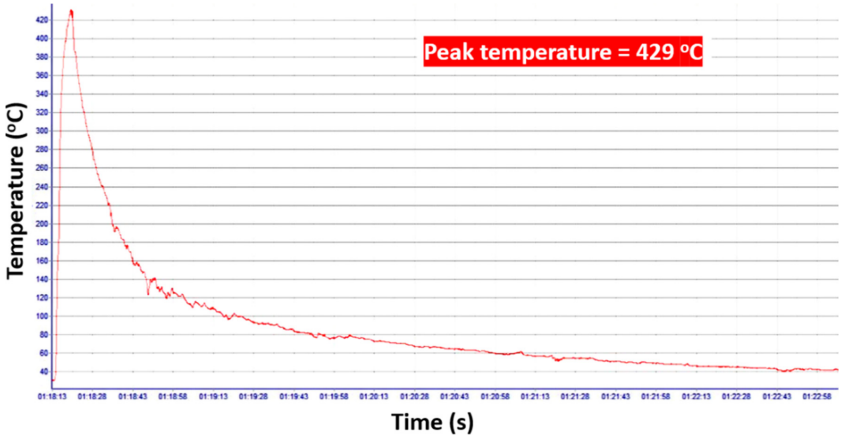

(a)

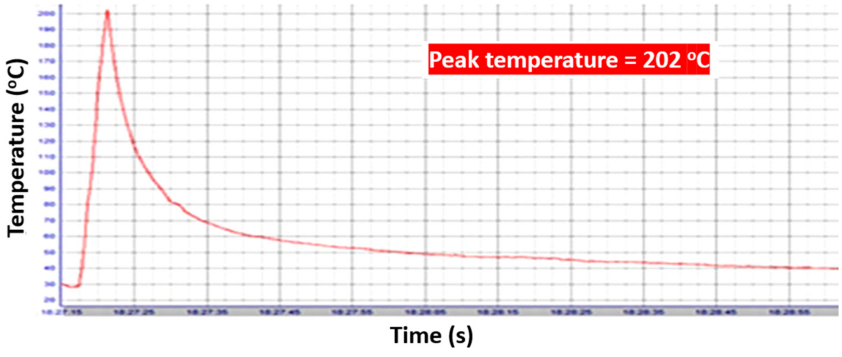

(b)

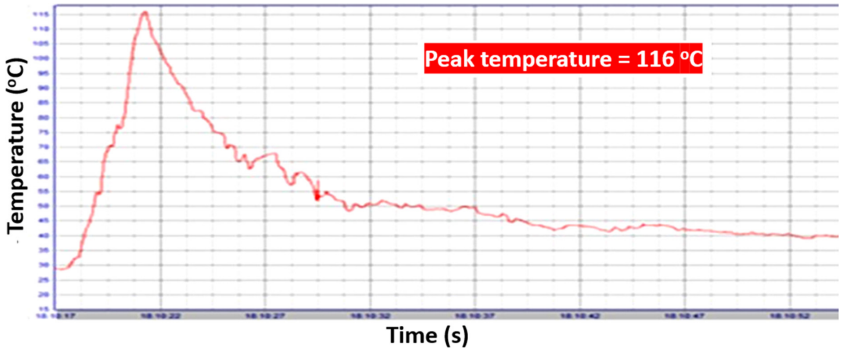

(c)

Fig. 7. (Color online) The experimental temperature profile of Al–MS. (a) Specimen 1, (b) specimen 2 and (c) specimen 3.

pressure and forging time were all adjusted at 1600 rpm, 300 kPa, 6 s, 500 kPa, and 8 s. Figures 7(a)–7(c) show the measured data for specimen 1, specimen 2 and specimen 3 plotted against time using Data Temp MX. The determination of peak temperature at the interface is critical during the friction stud welding process because it has a significant impact on the production of flash, heat-affected zone and welded joint strength.[31] A noncontact type infrared thermometer with a time period of 0.03125 s was used to take online temperature measurements at the joint interface. The experimental peak

temperature of friction stud welded Al–MS specimens is mentioned in Figs. 7(a)–7(c). It is observed that specimen 1 (interface distance $x = 0$) contains the highest temperature (429°C) and the results of temperature with respect to time are reduced subsequently (202°C and 116°C) for another specimen (2 and 3) that contains $x = 5$ and 10 mm interface. Therefore, it is concluded that the highest temperature is found in the zero interface of the Al–MS sample during the friction stud welding process.

4.2. *Effect of size of stud, the rotation speed of the spindle, friction pressure, and coefficient of friction on heat generation*

Figure 8(a) shows the effect of the size of the stud on heat generation. If the size of the stud is increased, the heat flux is also increased corresponding to the rotational speed from 800 rpm to 1600 rpm. Figure 8(b) shows the effect of speed of rotation on heat generation. If the rotational speed is increased, the heat flux is also increased corresponding to the frictional pressure from 200 kPa to 1000 kPa. Figure 8(c) shows the effect of friction pressure on heat generation. If the frictional pressure is increased, the heat generation is also increased corresponding to the rotational speed of the spindle. Figure 8(d) shows the effect of the coefficient of friction on heat generation. If the coefficient of friction is increased, the heat flux is also increased corresponding to the rotational speed from 800 rpm to 1600 rpm.

4.3. *Validation of the finite-difference model*

For validation of the FDM, the temperature profile generated by the analytical model is compared with

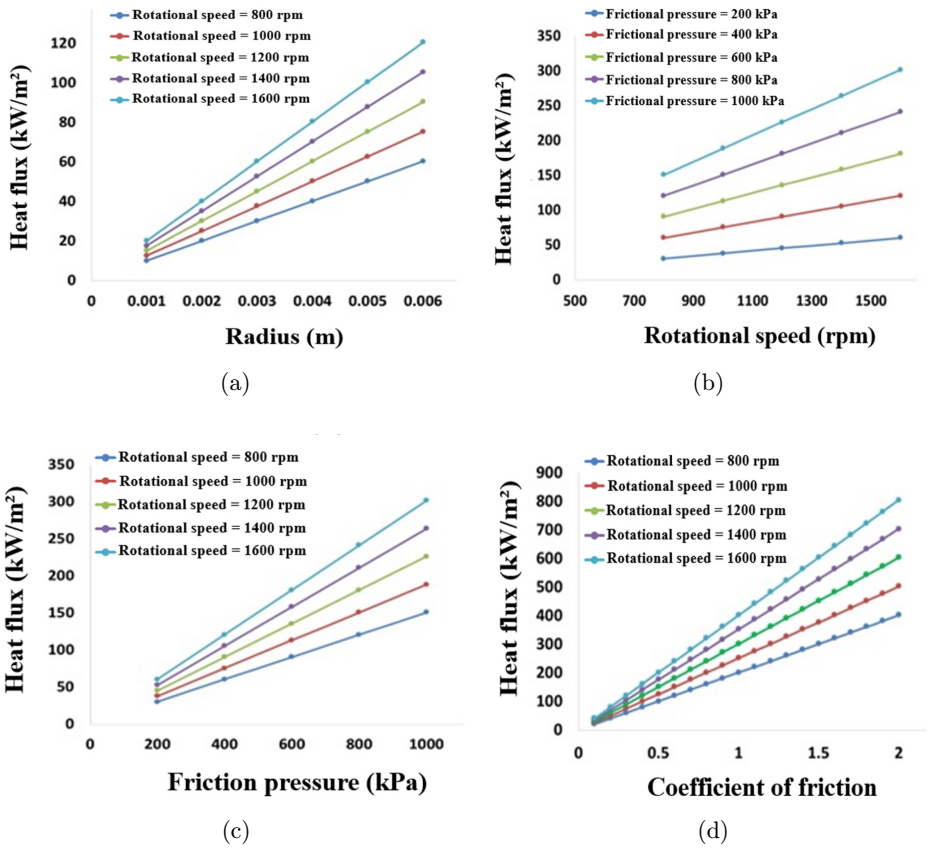

Fig. 8. (Color online) Effect of parameters on heat generation. (a) Stud size, (b) rotating speed, (c) friction pressure and (d) coefficient of friction.

the experimentally measured values. When compared with the measured data at a distance of 5 and 10 mm from the weld interface, the analytical values show fair agreement with the experimental values. The computed temperature profile is not exactly matching with the experimental data due to some errors, particularly in the cooling part. This is due to the zero axial shortening assumption in the FDM. During the actual friction stud welding process, the flash would be expelled out at every instant due to the relative movement of the rubbing components. But this relative movement of the two parts is not considered in the present model and so there is not a perfect match between the analytical results with the experimental results (Figs. 9 and 10). However, the trend of the two profiles shown is almost the same.

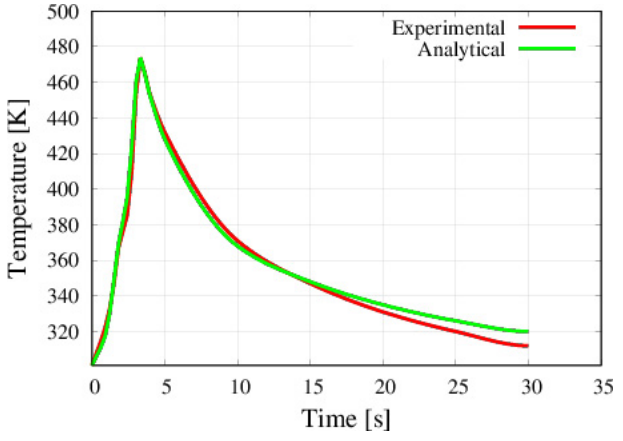

Fig. 9. (Color online) Time–temperature profiles at a distance of $x = 5$ mm from the interface of friction welded Al–MS specimen.

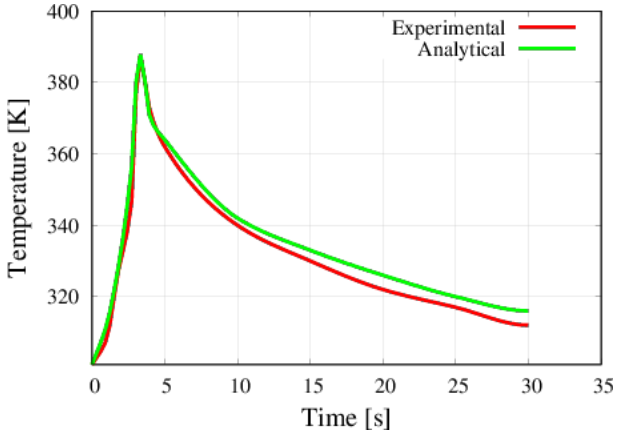

Fig. 10. (Color online) Time–temperature profiles at a distance of $x = 10$ mm from the interface friction welded Al–MS specimen.

4.4. *Prediction of thermal profiles*

Using the FDM, the time–temperature profile can be generated for any instant. Based on the obtained temperature distribution, the graphs are plotted between the length of the joint and the temperatures (Fig. 11). In all the graphs, the profile is broader on the Al side and narrower on the MS side. This is due to the change in the thermal properties of the dissimilar metals. The thermal conductivity of Al is higher than the thermal conductivity of MS. As a result, there is a high thermal gradient at the MS. So, the thermal profile is narrow at the MS and broader on the Al side. Thus, the knowledge of the temperature joint distribution could be helpful in calculating the microstructure evolution, the thermal cycle of the method, and residual stress formation.

4.5. *Numerical simulation*

The friction stud welding of Al and MS will be numerically modeled in this study using ANSYS. The study's goal was to consider temperature changes, temperature dispersion and heat transmission during the procedure. Both workpieces are 45 and 12 mm in length and diameter, respectively. The numerical simulation is run with the properties of the materials listed in Table 1. Quad 4 node plane 55 was chosen as the element type in ANSYS. Material properties for Al and MS have been provided. Meshing was completed. The components' boundary criteria were provided. Loads were applied to the components in a controlled manner. A transient analysis was performed. The outcomes of the problem can be obtained and plotted in the post-processor after it has been solved. The numerical modeling of Al–MS joints is shown in Fig. 12. There are 688 nodes created in this analysis. Figure 12(a) displays the finite element model and Figs. 12(b)–12(f) shows a contour plot of temperature distribution at various times (1–5 s) in which the temperature dissipation is shown to be greater in Al than MS due to Al's higher thermal conductivity.

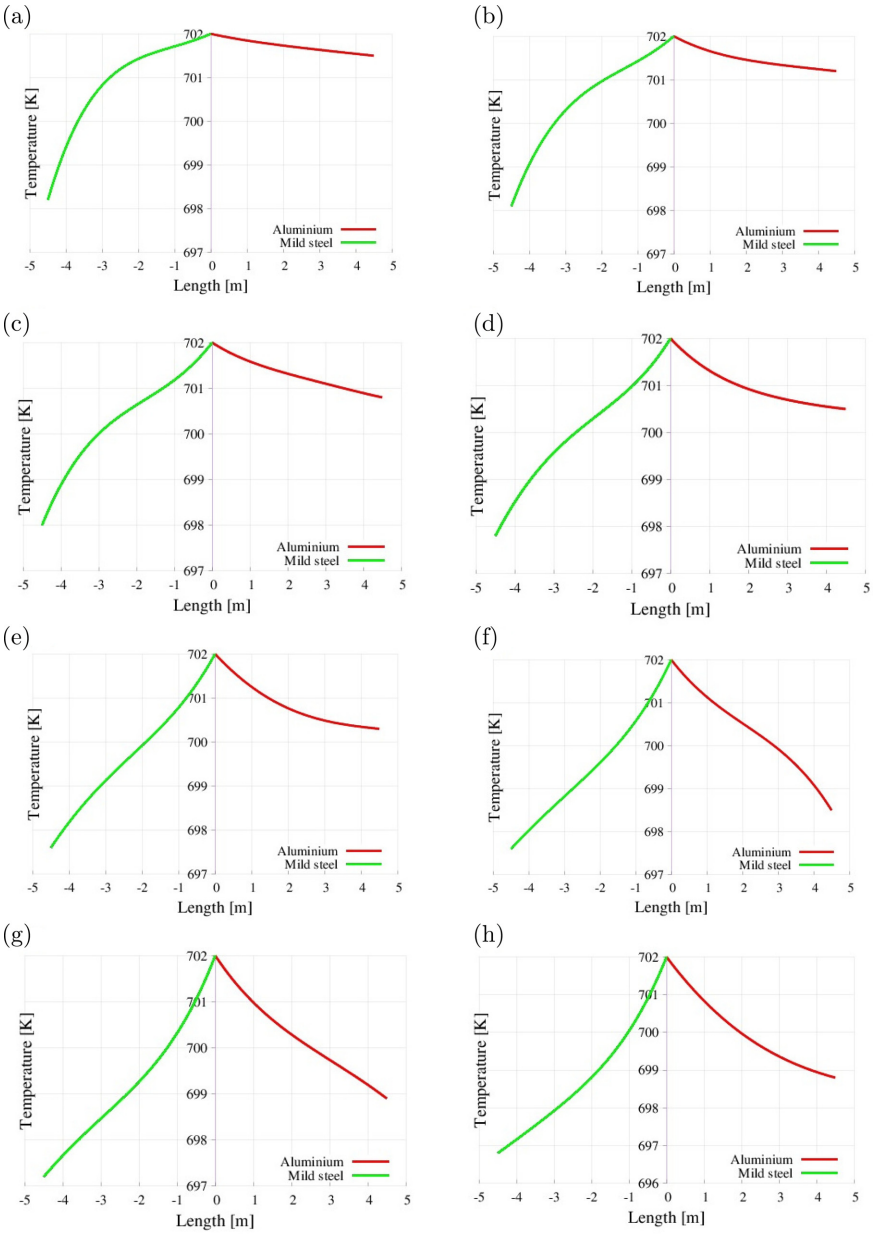

Fig. 11. (Color online) Predicted FDM thermal profile at different time. (a) 0.5 s, (b) 1 s, (c) 1.5 s, (d) 2 s, (e) 2.5 s, (f) 3 s, (g) 3.5 s and (h) 4 s.

5. Conclusion

In this study, friction stud welding of aluminum and mild steel combinations is carried out for various process parameters, such as frictional time, frictional pressure, rotational speed, forging pressure, and forging time. The important outcomes of this study are as follows:

- The heat generation at the interfacial area of the welded components is determined using a micro-annulus heat generation model. It was found that the generation of heat is varied by varying the stud size, rotational speed, friction pressure, and coefficient of friction during the process.
- The quality of the welded specimen is affected due to the temperature at the joint interface. So, the temperature distribution is determined using the thermal resistance and capacitance formulation of the FDM at transient conditions

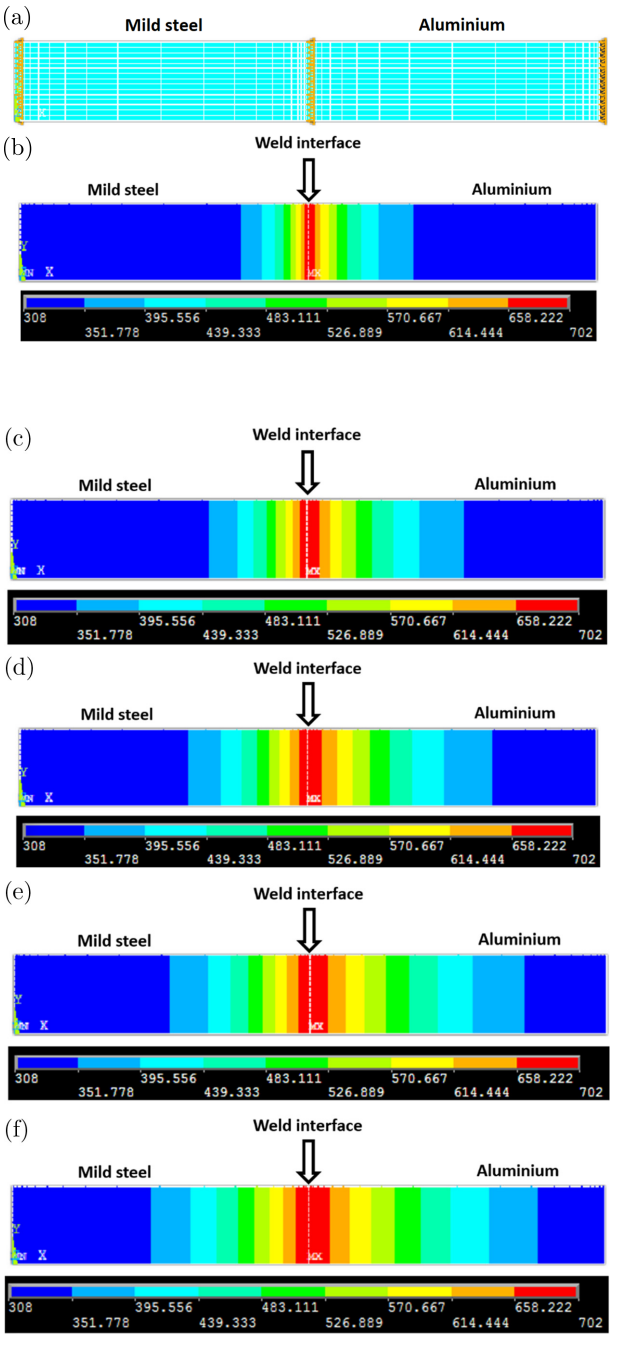

Fig. 12. (Color online) Numerical simulation plots. (a) Finite element model and temperature distribution at time (b) 1 s, (c) 2 s, (d) 3 s, (e) 4 s and (f) 5 s.

for 5 and 10 mm distance from the welded interface.

- The obtained temperature results are compared with the experimental results and found that the mathematical results are in good agreement with the experimental data on the heating side and fewer errors on the cooling side because of the zero-axial shortening assumption.
- ANSYS software was used to perform numerical simulations for the joining of dissimilar metals. Due to the thermal properties of the material, the temperature distribution for aluminum and mild steel was determined at various time increments, and it was found that the temperature distribution is more on the aluminum side compared to the mild steel side.

Acknowledgment

The authors gratefully acknowledge the financial support of SERB of the Department of Science & Technology, New Delhi (No. SERB/F/1452/2013-2014).

References

1. G. Çam, V. Javaheri and A. Heidarzadeh, *J. Adhes. Sci. Technol.* (2022) 1, https://doi.org/10.1080/01694243.2022.2028073.
2. A. Heidarzadeh, S. Mironov, R. Kaibyshev, G. Çam, A. Simar, A. Gerlich, F. Khodabakhshi, A. Mostafaei, D. P. Field, J. D. Robson, A. Deschamps and P. J. Withers, *Prog. Mater. Sci.* **117** (2022) 100752.
3. G. Ipekoglu and G. Cam, *Metall. Mater. Trans. A* **45** (2014) 3074.
4. Y. Ai, P. Jiang, X. Shao, C. Wang, P. Li, G. Mi, Y. Liu and W. Liu, *Mater. Des.* **90** (2016) 669.
5. N. R. J. Hynes, P. Nagaraj and J. A. J. Sujana, *Arab. J. Sci. Eng.* **39** (2014) 5017.
6. N. Kashaev, V. Ventzke and G. Cam, *J. Manuf. Processes* **36** (2018) 571.
7. G. Cam and G. Ipekoglu, *Int. J. Adv. Manuf. Technol.* **91** (2017) 1851.
8. G. Cam, *Int. Mater. Rev.* **56** (2011) 1.
9. G. Cam, G. Ipekoğlu and H. T. Serindag, *Sci. Technol. Weld. Join.* **19** (2014) 715–720.
10. G. Ipekoglu and G. Cam, *Metall. Mater. Trans. A* **45** (2014) 3074.
11. G. Cam and G. Ipekoglu, *Int. J. Adv. Manuf. Technol.* **91** (2017) 1851.
12. T. Kucukomeroglu, S. M. Aktarer, G. Ipekoglu and G. Cam, *Mater. Test.* **60** (2018) 1163.
13. G. Cam, V. Ventzke, J. F. dos Santos, M. Kocak, G. Jennequin and P. Gonthier-Maurin, *Sci. Technol. Weld. Join.* **4** (1999) 317.
14. G. Cam and M. Kocak, *J. Mater. Sci.* **42** (2007) 7154.
15. W. Ratanathavorn and A. Melander, *Sci. Technol. Weld. Join.* **20** (2015) 222.

16. N. R. J. Hynes, P. Nagaraj and J. A. J. Sujana, *Mater. Des.* **62** (2014) 118.
17. C. H. Muralimohan, M. Ashfaq, A. Rouholah, V. Muthupandi and K. Sivaprasad, *Metall. Mater. Trans. A* **47** (2016) 347.
18. T. Matsuda, H. Adachi, T. Sano, R. Yoshida, H. Hori, S. Ono and A. Hirose, *J. Mater. Process. Technol.* **269** (2019) 45.
19. N. Sharma, Z. A. Khan and A. N. Siddiquee, *Trans. Nonferrous Met. Soc. China.* **27** (2017) 2113.
20. M. Kimura, M. Kusaka, K. Kaizu, K. Nakata and K. Nagatsuka, *Int. J. Adv. Manuf. Technol.* **82** (2016) 489.
21. M. Sahin, *Ind. Lubr. Tribol.* **66** (2014) 260.
22. A. M. Sadoun, A. Wagih, A. Fathy and A. R. S. Essa, *Results Phys.* **15** (2019) 102814.
23. H. Seli, A. Ismail, E. Rachman and Z. Ahmad, *J. Mater. Process. Technol.* **210** (2010) 1209.
24. V. Pandian and S. Kannan, *J. Manuf. Processes* **54** (2020) 99.
25. H. A. Derazkola, A. Eyvazian and A. Simchi, *J. Manuf. Processes* **50** (2020) 68.
26. O. Gopkalo, X. Liu, F. Long, M. Booth, A. P. Gerlich and B. J. Diak, *Mater. Sci. Eng. A* **754** (2019) 205.
27. P. Jedrasiak, H. R. Shercliff, A. Reilly, G. J. McShane, Y. C. Chen, L. Wang, J. Robson and P. Prangnell, *J. Mater. Eng. Perform.* **25** (2016) 4089.
28. N. P. Patel, P. Parlikar, R. S. Dhari, K. Mehta and M. Pandya, *J. Manuf. Processes* **47** (2019) 98.
29. C. J. Cheng, *Welding J.* **41** (1962) 542.
30. C. J. Cheng, *Welding J.* **42** (1963) 233.
31. A. Moal and E. Massoni, *Eng. Comput.* **12** (1995) 497.
32. R. M. Selvaraj and N. R. J. Hynes, *AIP Conf. Proc.* **2142** (2019) 110006.
33. N. R. J. Hynes, P. Nagaraj and J. A. J. Sujana, *Exp. Tech.* **43** (2019) 491.
34. R. Tharmaraj, N. R. J. Hynes and P. S. Velu, *J. Braz. Soc. Mech. Sci. Eng.* **42** (2020) 538.
35. P. S. Velu, N. R. J. Hynes and N. J. Vignesh, *J. Braz. Soc. Mech. Sci. Eng.* **41** (2019) 537.
36. N. R. J. Hynes and P. S. Velu, *Mater. Res. Exp.* **6** (2019) 026573.
37. N. R. J. Hynes, P. Nagaraj and R. Tharmaraj, *Int. J. Appl. Eng. Res.* **10** (2015) 6107.
38. P. Karuppasamy, N. R. J. Hynes and J. A. J. Sujana, *Int. J. Appl. Eng. Res.* **9** (2014) 9028.
39. N. R. J. Hynes, P. Nagaraj and R. Tharmaraj, *Adv. Mater. Res.* **984** (2014) 592.
40. N. R. J. Hynes, P. S. Velu, R. Tharmaraj and R. Kumar, *AIP Conf. Proc.* **1728** (2016) 020550.
41. N. R. J. Hynes, R. Tharmaraj, P. S. Velu and R. Kumar, *AIP Conf. Proc.* **1728** (2016) 020556.
42. N. R. J. Hynes and R. Tharmaraj, *J. Therm. Eng. Appl.* **2** (2015) 22.
43. M. A. Ali, K. Ishfaq, M. H. Raza, M. U. Farooq, N. A. Mufti and C. I. Pruncu, *Int. J. Adv. Manuf. Technol.* **107** (2020) 3277.
44. B. Guo, Z. Zhang and R. G. Li, *NDT & E Int.* **93** (2018) 34.
45. R. Winiczenko, *Int. J. Adv. Manuf. Technol.* **84** (2016) 941.
46. M. Tisza and I. Czinege, *Int. J. Lightweight Mater. Manuf.* **1** (2018) 229.